From solar to hydrogen: Preliminary experimental investigation on a small scale facility

(Article begins on next page)

17 July 2024

# FROM SOLAR TO HYDROGEN: PRELIMINARY EXPERIMENTAL INVESTIGATION ON A SMALL SCALE FACILITY

**M. A. Ancona[1], M. Bianchi[1], L. Branchini[1\*], A. De Pascale[1], F. Melino[1], A. Peretto[1], J. Rosati[2], L. B. Scarponi[2]**

[1]Alma Mater Studiorum - Università di Bologna, DIN – viale del Risorgimento, 2, 40136 Bologna, ITALY
[2]Alma Mater Studiorum - Università di Bologna, CIRI-EA – via Angherà, 22, 47900 Rimini, ITALY

\*corresponding author, e-mail: lisa.branchini2@unibo.it, phone: +39-051-2093314

**ABSTRACT**

Issues of exhaustible natural resources, fluctuating fossil fuel prices and improvements in electric power systems motivated governments to behave positively toward the development of distributed generation. In addition, progresses in small size generation technologies and storage systems give rise to a significant diffusion in microgrids, working together with conventional power grid. Indeed, in the next future, domestic microgrids are expected to play a fundamental role in electric power networks, driving both the academic and industrial research interests in developing high efficient and reliable conversion and storage technologies.

In this context, this study presents a feasible configuration of a solar-hydrogen integrated microgrid and documents the procedure to characterize the overall efficiency of a laboratory scale test facility. Experimental results highlight that the most significant inefficiencies in the solar to hydrogen conversion process are mainly attributed to the solar to electrical energy conversion process, being responsible for about 89 % of losses. The overall laboratory scale solar to hydrogen chain can reach conversion efficiency up to 5.3 %.

**Keywords:** photovoltaic, hydrogen, battery, experimental setup, Stand-alone power system.

## 1. INTRODUCTION

The rational exploitation of renewable sources, the improvement in conversion efficiencies, the reduction of wasted energy and the minimization of pollutant emissions are the crucial purposes of any energy policy, whether applied at local, national or global level [1]. Distributed generation (DG) is one of the key strategies for achieving these goals [2]. DG plays a fundamental role also in rural areas, where power deliver over long distance is difficult and uneconomical [3]. In those areas, energy supply requirements must be guarantee taking advantage from stand-alone hybrid systems typically dependent on renewable sources [4]. As a consequence, a key role in the DG network is played by renewables and, in particular, by the non-programmable sources such as solar and wind [5, 6]. As known, the characteristics of non-programmable sources are adverse to the diffusion of renewable energy; in particular, intermittency presents a great challenge in energy generation and load balance maintenance to ensure power network stability and reliability [7-10]. Great efforts have been made in searching for viable

solutions, including Electrical Energy Storage (EES), load shifting through demand management, interconnection with external grids, etc. Among all, EES has been recognized as one of the most promising solution with a huge potential in meeting renewable challenges [11, 12]. In fact, in order to match final user needs with renewable sources energy generation, the presence of storage devices is of fundamental importance. According to generation technology and users needs, different EES systems can be used to store energy in the most efficient way. A deep review on EES state-of-art can be found in [13-20]. For small/micro size applications, among all EES devices, batteries are the most diffused solutions. Batteries are suitable for different applications, such as power quality, energy management, riding through power and transportation systems [19]. At present, research and development on batteries are mainly focused on: (i) new materials to improve performance, (ii) extending the useful life by increasing the maximum cycling rates, (iii) improving charging/discharging capabilities. Batteries integration, as electrical storage devices, with renewable sources (solar and/or wind) is fundamental for application in microgrids.

Several projects and research activities are currently focused on chemical storage and, in particular on the investigation of affordable approaches to extract large amounts of hydrogen from water by using renewable, non-programmable sources. Generated hydrogen through water electrolysis can be stored in canisters for later use in fuel cell for electricity and heat generation, thus resulting in combined heat and power technologies [19].

In this context and to perform experimental surveys on this topic, a new laboratory has been set-up by the Energy and the Environment Interdepartmental Centre for Industrial Research, CIRI-EA, of the University of Bologna at Ravenna Technopole. The "*microgrid and storage*" laboratory test facility is within the scope of the High Technology network of Emilia-Romagna. Present and future research activities are expected to define optimal operations and control strategies to exploit small scale renewable sources in a rational and effective way, also tanks to the use of different storage devices. The laboratory of integrated microgrid consists of solar photovoltaic panels (PV) for the exploitation of the renewable non-programmable source, batteries and a hydrogen generator (HG) as storage technologies, power electronics including inverter and converter, a solar charge regulation unit (SCR) and electronic load emulators, both direct (DC) and alternate current (AC), as users. The integrated microgrid is intended to maximize the hydrogen generation starting from a renewable source through the use of batteries to compensate for solar over/under-production.

## 1.1 Renewable and storage technologies for micro-size distributed generation: state of the art

The literature survey on this subject mainly accounts for mathematical and semi-empirical models on integrated systems, mostly focused on sizing optimization methods and management strategies, examples can be found in [21-29]. More in details, Castañeda et al. [21] presented a sizing method and different control strategies for the energy management of a stand-alone hybrid system based on photovoltaic solar panels, hydrogen subsystem and battery, dynamic modelled in the Simulink environment. Three different control strategies were applied, based on technical-economic aspects. Study results highlighted that the hybrid system assures reliable electricity supply for the stand-alone application. However, although the configuration was found technically feasible, from the economic point of view was proven as not competitive. Ipsakisa et al. [22] developed efficient power management strategies for a stand-alone hybrid system, currently in operation in Greece, made up of a photovoltaic array, a wind generators and an electrolyzer to store renewable surplus energy via hydrogen production. Simulation results, under specific weather conditions, showed that the operation of the integrated system involves a number of decisions regarding the management and use of power: renewables intermittency

causes a frequent start-ups and shut-downs of electrolyzer, frequently operated far from maximum efficiency conditions. Similar conclusions was found in [23] where Carpellucci and Giordano developed a simulation tool for evaluating the energy/economic performance of stand-alone integrated systems, including various electricity generation technologies (photovoltaic modules, wind turbines and micro-hydroelectric plants) and hydrogen storage devices. Zhoua et al. [24] applied to different case studies the proposed energy management strategy and system sizing method used to determine the minimum capacity of the system components. In details, their study analyzed an integrated system including PV panel, electrolyzer, hydrogen tank, fuel cell and battery. Their preliminary simulation results showed that the proposed methodology provides a good straightforward solution to the pre-design and operation of stand-alone PV-$H_2$ systems.

Guonit et al. in [25] described a technical-economic study of a PV-hydrogen-battery hybrid system for off-grid power supply taking into account the impact of performances' ageing on optimal system sizing. Study's novelty mainly lies in the simultaneous optimization of the power management strategy and the components' size, performing a detailed modelling of the components (power consumption of the auxiliaries and ageing approach in the form of performances degradation). Results confirmed the interest of hybridizing batteries with a hydrogen system, compared to PV-batteries solution. Despite its investment cost, the limited size of hydrogen chain is sufficient to reduce the need for large and costly battery energy storage capacity. The performed sensitivity analyses on battery bank and hydrogen chain costs showed that the PV-Batteries-H2 solution is more profitable than the PV-Batteries configuration even if the cost of the battery bank decreases. Moreover, results also showed the limited impact of the hydrogen chain capital costs.

Tesfahunegn et al. [26] analyzed different management strategies for the optimum operation of an integrated system composed of PV panels, batteries, an electrolyser and fuel cells (FC). A simulation study using SIMULINK/SIMPOWER is conducted, based on realistic irradiance data relative to the Oslo (Norway) area. The batteries are used when the required power is higher than that provided by PV panels and FC. The results show that FC and electrolyser work under more favorable conditions so their life time increases.

Niasati and Behzadi [27] considered a system configuration similar to the one described above, but they took into account also the hydrogen level in the storage tank for the power management strategy. In their study, three different methods are analyzed using TRNSYS software.

Ulleberg has developed control strategies, simulated in TRNSYS, tested and verified against a reference represented by PHOEBUS plant in Jülich, Germany [28]. The study highlighted that the performances of a PV-Hydrogen system significantly depend on control strategies. To find an optimum, a techno-economic analysis, that takes into account both control strategies and size of the system components, has to be performed.

Clark et al. [29] studied a direct coupling of PV panels, with maximum power output equal to 2.4 kW, and a Proton Exchange Membrane (PEM) electrolyser. The proposed configuration allows to minimize the interfacing control and power electronics; in this way the costs of a DC/DC converter can be avoided. The overall solar to hydrogen energy conversion efficiency is rated about 4.7 %.

In details, the use of the non-dispatchable renewable energy sources (wind and photovoltaic) and their combination with short-/long-term electricity storage options for off-grid and grid connected systems are subject to many publications. In the contest of distributed generation, applications of renewable sources with hydrogen generation technologies can be found in [30-36]. In particular, Dursum et al. investigated a dynamic model for hydrogen production fed by a stand-alone renewable hybrid power system. The model developed with MATLAB/Simscape considers a PEM electrolyzer powered by a 1 kW wind turbine and a PV arrays with nominal

installed power equal to 1.8 kW. The calculated hydrogen annual production is 34.4 kg. The differences between model and real data are quantified with mean square error and the result is $8.28 \cdot 10^{-7}$ [30]. Eroglu et al. described a mobile renewable house consisting of an 800 W PV panels, a 1 kW wind turbine and a 2 kW fuel cell. The PV panels and the wind turbine are connected to 8 gel type batteries of 200 Ah at 12 V. The annual energy production of the mobile house is 2510 kWh while the annual demand is 1550 kWh. The energy surplus is converted into hydrogen by means of a PEM electrolyzer and stored in pressurized tanks to feed the fuel cell when it is necessary [31]. Santarelli et al. described the design and analysis of stand-alone hydrogen energy systems with different renewable sources (wind, solar and hydraulic energy). The system is designed to satisfy the demand of a residential user. In all the analyzed cases, the annual efficiency of the hydrogen production chain keeps close to 38 % [32]. Escobar et al. reported an analytical model for the sizing of a hydrogen production system based on renewable energy which, as test case study, was applied to the Mexican Caribbean area. The system consist of PV panels, a wind turbine, electrolyzer and fuel cell and takes advantage devices experimental data for wind speed and solar radiation. The results show that the highest values of nominal power do not always lead to highest efficacy of the hybrid system. Through the   use of the proposed analytical model is possible to size the integrated system and to select the most appropriate control strategy [33]. Sanchez et al. performed a techno-economic optimization based on optimization algorithm for a stand-alone wind-photovoltaic-hydrogen power system placed at south-east region of Mexico. The study has the aim of sizing the integrated system, which has to satisfy the power demand of an isolated residential load. The model employs the Particle Swarm Optimizer algorithm to find the optimal solution that leads to system minimum cost. The optimal configuration consists of 17 photovoltaic modules (180 W each), 4 kW wind turbine, 3 kW fuel cell and 3 kW electrolyzer. The total cost results close to 3700 dollars assuming 20 years of operation [34]. L. G. Arriaga et al. reported a direct coupling of a 2.7 kW solar panel system with a solid polymer electrolyte electrolyzer in Mexico.   The complete electrolyzer (stack plus auxiliaries) has a maximum hydrogen production of 1000 normal liters per hour, with a power consumption of   8 kVA. The results show that the direct coupling, with solar radiation in the range of 600÷800 $W/m^2$, is possible with a correct design of the PV arrays [35]. Finally, Yunez-Cano et al. [36] detailed a model to size and evaluate the feasibility of a photovoltaic- hydrogen energy integrated system applied to a 24 square meters isolated mobile house. The system consists of PV panels, an electrolyzer and a fuel cell. The panels feed the electric load and the excess energy is converted in the electrolyzer to generate hydrogen. The latter is used by the fuel cell when the energy provided by the panel results insufficient to satisfy the load. The proposed analytical method allows to size the hybrid system in order to achieve the highest conversion efficiency.

## 1.2 Experimental research contribute to literature

In this contest, the main contribution of this work with respect to literature is the laboratory size scale analyzed and the performance evaluation of the integrated system on the basis of experimental results. In particular, in contrast with [21, 26, 27], the configuration presented in this paper does not include a fuel cell; only the SOC of the batteries is controlled by means of the solar charge unit. The main objective is the hydrogen production: for this reason the PEM electrolyser has the priority with respect to batteries, the available power is primarily directed to it. Furthermore, the functioning of the system is analyzed without an external load. Only the power required by the auxiliaries is either subtracted to that produced by PV panels or stored in the batteries. Another peculiarity of this work is represented by the calculation of the efficiencies of every component, allowing to evaluate the different types of the system losses. Authors presents different experimental tests carried out in

order to investigate system components interaction. In particular, the presence of a solar charge regulation unit, used to control the power coming from the PV modules and directed to batteries, is analyzed. PV operating conditions and performance during batteries charging/discharging process are analyzed and compared to Maximum Power Point (MPP) conditions. Experimental results will provide preliminary information on microgrid components average conversion efficiency and of the overall solar-hydrogen generation chain. On the basis of the integrated system operation, the most critical components will be identified and improvements on the solar-to-hydrogen conversion process will be suggested.

The paper is structured as follows: Section 2 shows the laboratory integrated microgrid layout with detailed description of main components. Section 3 presents a schematic of energy fluxes involved in the charging/discharging processes and defines components conversion efficiency. The experimental results for single microgrid components are presented and discussed in Section 4, while, in Section 5 the overall solar-hydrogen generation chain efficiency is evaluated. Finally, conclusion are given in Section 6.

## 2. MICROGRID DESCRIPTION

Schematic layout of the current installation, including measuring sensors, is illustrated in Fig. 1. The laboratory integrated microgrid (pictures can be found in Fig. 2) accommodates the following components:

- − two solar PV modules parallel connected;
- − a power management cabinet including a solar charge regulator unit, two batteries, a DC/DC converter and a DC/AC inverter (24 V/230 V);
- − a Hydrogen Generator (HG) equipped with an internal AC/DC rectifier and three hydrogen storage metal canisters.

The microgrid is also equipped with a solar emulator (SE) and a DC electronic load emulator as indicated in Fig. 1. The test bench is endowed with sensors for current (IR), voltage (ER), temperature (TR), solar radiation (RR) , mass flow rate (QR) and water quality (LR) (Fig. 1 ); measured data are sent to a data acquisition system device.

### *Solar Modules*

Solar energy is converted into electrical energy through the polycrystalline photovoltaic arrays. The PV panels are connected in parallel and located on movable racks with an adjustable tilt angle so that they can be positioned facing various directions. A sensor kit, which includes a pyranometer, (Fig. 1) is connected to the PV solar arrays for the recording of environmental temperature (TR1 in Fig. 1), modules temperature (TR2 in Fig. 1) and solar radiation (RR1 in Fig. 1). Each of the solar modules delivers up to 220 W with rated voltage equals to 24 V. Detailed solar modules specifications are presented in Table A1, Appendix A. Efficiency of the solar modules at standard conditions (STC: Radiation 1000 $W/m^2$ with a spectrum of AM 1.5 at a cell temperature of 25 °C) is rated to 15%. Based on manufacturer data, when operated at nominal operating cell temperature (NOCT: Radiation 800 $W/m^2$, ambient temperature of 20 °C and a nominal operating cell temperature of 48°C) the solar module performance are reduced down to 155 W [37]. Based on manufacturer specifications (see Table A1 Appendix A), Fig. 3 shows I-V curves (with short circuit current, $I_{SC}$, and open circuit voltage, $V_{oc}$) and maximum power point (MPP) values at STC and NOCT conditions. The value of MPP voltage, $V_{MPP}$, and current, $I_{MPP}$, are 27.54 V and 8.08 A when the modules operate under STC condition and 23.40 V and 6.62 A, respectively, when the modules operate at NOCT condition [30].

200

*Solar Charge Regulator*

Charge acceptance is a term often used to describe the efficiency of battery recharging process. Since solar batteries are constantly recharged with a limited energy source (e.g. opportunity to charge with available sunlight), a high charge acceptance is a critical issue for the required reserve capacity and performance.

Charging a battery through a PV module without a regulation device has to be avoided because it can damage battery itself and shortening its life cycle. In practice, a DC/DC converter is necessary to regulate and provide suitable charging voltage/current according to the battery specifications. Several types of charge controller units can be used, as specified in [38]. Moreover, the job of the solar charge controller is to regulate the power going from the solar panels to the batteries. The key controller protection functions are: overcharge and deep discharge protection; reverse polarity and reverse current protection, short circuit protection; overvoltage protection; open circuit protection without battery; over-temperature and overload protections [39].

The most common approaches for charge controllers are Pulse Width Modulation (PWM) and Maximum Power Point Tracking (MPPT) charge controllers [40]. PWM is often used as a float charging method: the controller constantly checks the state of the battery to determine how fast to send pulses and how long (wide) the pulses will be. The controller monitors various battery parameters (V, I) during normal operation and uses this information to calculate the SOC of the battery. This type of controller allows the batteries to be more fully charged with less stress on the battery and by extending their life [39].

On the contrary, a MPPT controller device performs battery charging keeping PV panels close to maximum power point conditions for given incident solar radiation and weather conditions. In particular, a MPPT controller adjusts the operating point of a PV module extracting the highest possible instant power, thus increasing PV conversion efficiency [38]. A PWM controller is less expensive than a MPPT and represents a good trade-off choice for small systems; moreover, performance advantage of MPPT controllers is significant, in particular, when the solar cell temperature is low (below 45 °C) or very high (above 75 °C) or when irradiance is very low [29]. The charging controller installed at the laboratory is a PR 3030 unit (Fig. 1) performing batteries charging through the PWM system, detailed specifications in Table A2, Appendix A [39]. The rated end of charge voltage for the PWM-PR 3030 is equal to 28.2 V with a rated module load current equals to 30 A and an own consumption of 12.5 mA.

*Batteries*

Two solar lead-acid batteries, working in series, are located inside the power management cabinet to store renewable energy of solar panels. The Banner Stand by Bull Block (Fig. 1) are closed, valve-regulated lead batteries with gelled electrolyte located in the fleece. Batteries voltage is rated 12 V each (thus, 24 V is the nominal voltage of series connection) while single battery capacity is rated 55 Ah. Complete specifications are presented in Table A3, Appendix A [41].

*DC/DC Converter and DC/AC Inverter*

The DC/DC converter (Fig. 1) feeding the DC electronic load is a Meanwell SD-25B-12 converting 24 V DC voltage from batteries to 12 V DC load [42].

The DC/AC Inverter (Fig. 1) feeding the Hydrogen generator is a Meanwell TS-700-224B converting 24 V DC voltage from batteries to 230 V AC voltage to HG[42]. Converter and inverter detailed technical data are listed in Table A4, Appendix A [42].

*Hydrogen Generator HG30 and Metal Hydride Canisters*

240  The hydrogen generator HG 30 (Fig. 1) enables the production of high-purity hydrogen by taking advantage of

241  PEM technology, in combination with an innovative gas dehydration system. The system is suitable for direct

242  operation with fuel cell systems or for filling low-pressure metal hydride canisters. By being connected with the

243  DC/AC inverter, the HG is equipped with an internal AC/DC rectifier. Pure hydrogen generation is rated 30 sl/h at

244  10.5 bar and, at the present, is stored into three metal hydride canisters (Fig. 1) with a capacity equals to 760 sl

245  each [43]. Technical specifications of HG and metal hydride canisters for hydrogen storage are summarized in

246  Table A5, Appendix A.

247  **3. ENERGY FLUXES AND COMPONENTS EFFICIENCY DEFINITION**

248  Fig. 4 shows a schematic of the charging (Fig. 4a) and discharging (Fig. 4b) tested process (highlighted with

249  continuous blue lines in figures). The charging process (Fig. 4a) consists in directing the solar radiation energy, $E_{RR}$,

250  converted by PV modules, $E_{PV}$, to batteries by means of the solar charge regulator unit. A constant fraction of

251  energy out from SCR unit is used to feed power management, cabinet auxiliaries and internal consumptions, $E_{aux}$,

252  while the remaining part, $E_{scr,out}$, is directed to batteries, $E_{b,in}$. Once batteries are completely charged, PV are

253  disconnected and energy stored is discharged (Fig. 4b), $E_{b,out}$, directing it to the DC/AC inverter, $E_{inv,out}$, and, later

254  on, to the HG unit, $E_{HGr,in}$, generating hydrogen, $E_{H2}$, stored into the metal canisters.

255  Based on notation in Fig. 4 a and b, each component can be characterized by a conversion efficiency.

256  PV panels efficiency, $\eta_{PV}$, is expressed by Eq. 1 as the ratio between the total energy output, $E_{PV}$, (see Fig. 4a)

257  and the total energy input, $E_{RR}$ (see Fig. 4a), evaluated as time integrals of output and input PV power,

258  respectively:

259
$$\eta_{PV} = \frac{\int_0^t P_{PV}\,dt}{\int_0^t P_{RR}\,dt} = \frac{\int_0^t P_{PV}\,dt}{\int_0^t RR \cdot S_{PV}\,dt} = \frac{E_{PV}}{E_{RR}} \tag{1}$$

260  where RR represents the solar radiation value [W/m$^2$] and $S_{PV}$ is the overall PV modules collecting surface [m$^2$]

261  (see Table A1, Appendix A).

262

263  The solar charge regulator efficiency, $\eta_{SCR}$, is defined as the ratio between the total energy output, $E_{SCR,out}$, and

264  the total energy input coming from PV panels, $E_{PV}$, as in Eq. 2:

265
$$\eta_{SCR} = \frac{\int_0^t P_{SCR,out}\,dt}{\int_0^t P_{PV}\,dt} = \frac{E_{SCR,out}}{E_{PV}} \tag{2}$$

266

267  Batteries charging/discharging efficiency, $\eta_B$, expressed, according to Eq. (3), as the ratio between the total

268  energy output, $E_{b,out}$, (to DC/AC inverter, see Fig. 4 b) and the total energy input, $E_{b,in}$, (from solar charge unit see

269  Fig. 4 a):

270 $$\eta_B = \frac{\int_0^t P_{b,out} dt}{\int_0^t P_{b,in} dt} = \frac{E_{b,out}}{E_{b,in}}$$ (3)

271

272

273 The efficiency of the inverter, $\eta_{DC/AC}$, is expressed as the ratio between the total energy output, $E_{HG,in,}$ and the

274 total energy input , $E_{INV}$, as in Eq. (4):

275 $$\eta_{DC/AC} = \frac{\int_0^t P_{HG,in} dt}{\int_0^t P_{INV} dt} = \frac{E_{HG,in}}{E_{INV}}$$ (4)

276

277 The efficiency of the HG+AC/DC component, $\eta_{HG-AC/DC}$, is defined as the ratio between the total energy output

278 stored into metal canisters, $E_{H2}$, (evaluated as product of hydrogen mass flow rate and Higher Heating Value,

279 HHV) and the total energy input to the HG, $E_{HG,in}$, according to Eq. (5):

280

281 $$\eta_{HG-AC/DC} = \frac{\int_0^t m_{H_2} \cdot HHV_{H_2} dt}{\int_0^t P_{HG,in} dt} = \frac{\int_0^t m_{H_2} \cdot HHV_{H_2} dt}{\int_0^t P_{HG,in} dt} = \frac{E_{H_2}}{E_{HG,in}}$$ (5)

282

283 **4.  EXPERIMENTAL RESULTS**

284 In order to characterize the photovoltaic panels feeding batteries during a charging process, experimental data

285 are presented and discussed. As example, Fig. 5 a-e show recorded solar radiation, RR in Fig. 5a, PV voltage, in Fig.

286 5b, PV current, in Fig. 5c, and calculated variables i.e. PV power output, Fig. 5d, PV efficiency, Fig. 5e, during

287 batteries charging process as a function of the time step. The time step of the acquisition system is 5 seconds. The

288 test was carried out during a springtime day with panels facing south and a tilt angle of 30 °, the laboratory is

289 located in Ravenna (latitude 44°25'4" North and longitude 12°11'58" East, 9 m above the sea level). Recorded

290 radiation values during the test are, most of the time, between 800 and 900 W/m$^2$ (see Fig. 5a) with an increasing

291 trend during test time. As previously detailed, PV power output is directed to batteries trough the operation of

292 SCR unit operated with PWM method. Based on measured solar radiation values and PV characteristics (see Fig.

293 3) it is possible to estimate current ($I_{MPP}$, Fig. 5c), voltage ($V_{MPP,}$ Fig. 5b), power output ($P_{MPP,}$ Fig. 5d) and efficiency

294 ($\eta_{MPP,}$ Fig. 5e) that solar modules would generate if the maximum power point conditions were pursued.

295 Comparing the data, for each aforementioned variables, it is possible to note that experimental PV operation

296 differs from theoretical MPP condition. The use of SCR to manage PV modules power output directed to batteries

297    causes the solar modules to operate quite far from maximum power point and, consequently, maximum

298    conversion efficiency. PV efficiency decreases down to 9 %, losing 6 percentage points on the respect of $\eta_{MPP}$

299    values, when batteries are about to be fully charged (see Fig. 5e).

300    As a confirm, Figure 6 compares several recorded experimental value of PV efficiency for different ambient

301    conditions (i.e. solar radiation values with constant values of ambient and PV cell temperatures) with PV

302    efficiency estimated based on MPP condition (calculated according to I-V curves in Fig. 3). Figure highlights that

303    through the use of a PWM regulation unit, depending on batteries SOC, solar panels are, most of the times, used

304    quite far from maximum power point conditions; furthermore, for a given value of solar radiation, different values

305    of PV efficiency are recorded, depending on batteries status.

306    Fig. 7 shows $\eta_{PV}$ values obtained in five experimental tests. Recorded values are in the range 10.0-14.5 %.

307    Compared to MPP efficiency values (see Fig. 7), a significant gap can be observed, in particular for tests #1 and #2,

308    where difference can achieve up to 5 percentage points. While, in case of test #5, as suggested by results, PV

309    modules have been operated close to MPP condition reaching 14 % of conversion efficiency.

310    In order to investigate PV efficiency results among tests, a detailed analysis of the recorded data has been carried

311    out. No significant differences have been recorded among experimental test in terms of ambient temperature

312    and solar modules' cells temperature; thus, reason for PV efficiency results must be sought in PV operation versus

313    MPP conditions. For each experimental test, average value of $I_{MPP}/I$, $V_{MPP}/V$, $P_{MPP}/P$ have been calculated along

314    with standard deviation and variance (see Table A6 in Appendix A). Standard deviation and variance results

315    confirm that during test #1 and #2 solar modules operate far from MPP conditions. In opposition, during test #5,

316    MPP condition is pursued.

317    Moreover, focusing on Figure 8 where PV efficiency values are plotted against voltage for two different values of

318    solar radiation (1000 and 800 W/m$^2$ ), it can be noticed that: increasing batteries charging voltage, the difference

319    between PV experimental efficiency and MPP values (red points in figure) increases, decreasing the solar

320    radiation value. Indeed, during test #1 and #2, characterized by significant efficiencies gap (see Fig. 7), low values

321    of RR (down to 500 W/m$^2$) have been recorded. On the contrary, test #5, recorded solar radiation values always

322    higher than 900 W/m$^2$.

323

324    *Solar Charge Regulator*

325    Different tests have been carried out in order to characterize the solar charger unit. The results obtained

326    demonstrate that the performance of the device are not affected by the operating conditions (solar radiation,

327    ambient temperature, batteries SOC, etc.). Therefore, the component is characterized by a constant efficiency

328    higher than 99 %.

329

330    *Batteries*

331    Fig. 9a shows the input/output power to/from the batteries recorded during a charging/discharging test (positive

332    and negative values respectively in figure). Fig. 9b shows corresponding batteries SOC during the test. At the

333    beginning of the test the batteries had the minimum allowed level of energy; in order to prevent degradation of

334    the batteries the SCR regulator avoids complete discharge by activating the deep discharge protection for SOC

335 below 30 %: voltage value at which disconnection occurs is around 22.2 V. At the end of the charging process

336 voltage is equal to 28.2 V: higher voltage values are not allowed by the SCR unit which stops the storage to

337 prevent overcharging and starts dissipating.

338 According to PV modules and solar charge characterization, dedicated tests have been carried out in order to

339 characterize batteries charging/discharging efficiency: Fig. 10 shows the calculated values. Obtained values, in the

340 range between 81 and 93 %, highlight that batteries efficiency can be subject to variations depending on initial

341 and final SOC. Additional tests will be carried out in the next future in order to have a deep characterization of

342 batteries return efficiency.

343

344 *DC/AC Inverter*

345 The input power to the DC/AC inverter unit comes from the gel batteries located inside the power management

346 cabinet while the output power is directed to the HG unit.

347 Obtained efficiency results show limited differences among tests, highlighting that the component is

348 characterized by an average value of conversion efficiency equal to 81.4 %.

349

350 *Hydrogen generator and AC/DC rectifier*

351 Finally, focusing on the HG unit, experimental tests have been performed in order to characterize HG operation

352 and its conversion efficiency in terms of generated hydrogen.

353 With reference to Fig. 1 and Fig. 4, it is possible to observe that the DC current output from the batteries is

354 converted into AC current through the inverter unit and then again into DC current through the AC/DC rectifier

355 located inside the HG device. Clearly, the output energy from the AC/DC rectifier equals the HG input energy (see

356 Fig. 4).

357 The recorded $\eta_{HG-AC/DC}$ values during HG operation are shown in Fig. 11 as function of input power. Obtained

358 experimental values show a parabolic trend increasing with the increase of input power till a maximum value,

359 close to 47 %, near 200 W. For higher input power values, component efficiency starts to decrease.

360

361 In order to characterize HG component in terms of conversion efficiency, five tests have been carried out and

362 results are shown in Fig. 12. From figure, it can be observed that there are no notable differences between tests:

363 HG+AC/DC operates close to its maximum conversion efficiency.

364

365 **5. SOLAR-HYDROGEN GENERATION CHAIN EFFICIENCY**

366 Once microgrid main components have been characterized, the overall solar-hydrogen generation chain efficiency

367 can be evaluated. Fig. 13 shows a schematic representation of the process with conservative assumptions i.e

368 minimum PV and Batteries efficiency values. The overall solar-hydrogen generation chain efficiency, $\eta_{Chain}$, can

369 be expressed as the product of each component efficiency as in Eq. (6):

370

371 $$\eta_{Chain} = \eta_{PV} \times \eta_{SCR} \times \eta_B \times \eta_{DC/AC} \times \eta_{HG-AC/DC} \tag{6}$$

372

373 Based on components behavior and above discussion, depending on PV and batteries efficiency values, the

374 overall $\eta_{Chain}$ can achieve from 3.4 up to 5.3 %.

375 As described in experimental results section, most important inefficiency in the solar-to-hydrogen generation

376 process has been identified in PV operations far from MPP conditions. Other issue (see Fig 4 b) lies in the

377 unnecessary DC/AC and AC/DC conversion processes between the solar charge and the HG unit. This double

378 conversion causes an energy loss that should be avoided in order to maximize the overall efficiency of the

379 process.

380


381 **6. CONCLUDING REMARKS**

382 The study presents the experimental integrated microgrid set up by the University of Bologna at Ravenna

383 Technopole. The microgrid is intended to generate pure hydrogen starting from solar radiation. The main

384 components of the solar-to-hydrogen generation chain are two photovoltaic solar panels connected in parallel,

385 two gel batteries connected in series as electricity storage device, a hydrogen generator and three metal

386 canisters for hydrogen storage.

387 A preliminary experimental activity has been carried out to characterize the main components and their

388 interaction within the microgrid in order to obtain a complete representation of the overall solar-to-hydrogen

389 generation chain. Main microgrid components experimental behaviors have been presented and discussed.

390 Results show that while the average efficiencies of the solar charge regulator, AC/DC inverter and hydrogen

391 generator do not show sensible variation from one test to the other, batteries and solar modules conversion

392 efficiencies depend on operating conditions. In particular, comparing the PV experimental operation versus

393 maximum power point condition, it has been observed that the use of solar charge regulation unit cause the

394 photovoltaic modules to operate quite far from maximum power and efficiency conditions.

395 Based on experimental tests, the overall solar-to-hydrogen chain efficiency ranges between 3.4 and 5.3 %.

396
397

398

**NONMENCLATURE**

*Acronyms*

| | |
|---|---|
| AC | Alternating Current |
| DC | Direct Current |
| DG | Distributed Generation |
| EES | Electrical Energy Storage |
| ER | Voltage |
| FC | Fuel Cell |
| HG | Hydrogen Generator |
| IR | Current |
| LR | Water Quality |
| MPP | Maximum Power Point |
| MPPT | Maximum Power Point Tracking |
| NOC | Nominal Operating Condition |
| PEM | Proton Exchange Membrane |
| PV | Photovoltaic |
| PWM | Pulse Width Modulation |
| QR | Mass Flow Rate |
| RR | Solar Radiation |
| SE | Solar Emulator |
| SCR | Solar Charge Regulator |
| SOC | State Of Charge |
| STC | Standard Condition |
| TR | Temperature |

*Greek symbols*

| | |
|---|---|
| $\eta$ | Efficiency [-] |

*Symbols*

| | |
|---|---|
| E | Energy [Wh] |
| HHV | Higher Heating Value [kJ/kg] |
| I | Current [A] |
| IR | Solar Irradiance [W/m$^2$] |
| m | mass flow rate [kg/s] |
| P | Power [W] |
| S | Surface [m$^2$] |
| V | Voltage [V] |

*Subscripts*

| | |
|---|---|
| aux | Auxiliary |
| B | batteries |
| H$_2$ | Hydrogen |
| in | Inlet |
| INV | Inverter |
| OC | Open Circuit |
| Out | Outlet |
| Net | Network |
| SC | Short Circuit |

**REFERENCES**

[1] "Directive 2009/28/EC of the European Parliament and of the Council of 23 April 2009 on the promotion of the use of energy from renewable sources and amending and subsequently repealing Directives 2001/77/EC and 2003/30/EC". Available at http://eur-lex.europa.eu/legal-content/en/ALL/?uri=CELEX:32009L0028

[2] A.A. Bayod-Rujula, Future development of the electricity systems with distributed generation, Energy, vol. 34 , 2009, pp. 377–383

[3] M. Bianchi, L. Branchini, A. De Pascale, A. Peretto, Application of environmental performance assessment of CHP systems with local and global approaches, Applied Energy, Vol. 130, 2014, pp. 774–782, Doi:10.1016/j.apenergy.2014.04.017

[4] A.M. Abd-el-Motaleb, Sarah Kazem Bekdach, Optimal sizing of distributed generation considering uncertainties in a hybrid power system, International Journal of Electrical Power & Energy Systems, Vol. 82, 2016, PP. 179–188, doi: 10.1016/j.ijepes.2016.03.023

[5] M. Bianchi, L. Branchini, C. Ferrari, F. Melino, Optimal sizing of grid-independent hybrid photovoltaic–battery power systems for household sector, 2014, Applied Energy, Vol. 136, 2014, Pages 805–816, Doi:10.1016/j.apenergy.2014.07.058

[6] M.A. Ancona, M. Bianchi, L. Branchini, A. De Pascale, F. Melino, A. Peretto, "Generation Side Management In Smart Grid", Proceedings of ASME ATI-UIT Conference on Thermal Energy Systems: Production, Storage, Utilization and the Environment 2015.

[7] L. Branchini, H. Perez-Blanco, Handling Wind Variability Using Gas Turbine, Proceedings of ASME Turbo Expo 2012, June 11-12, 2012, Copenhagen, Denmark, Vol. 6, 2012, pp. 727-734, Doi:10.1115/GT2012-68045

[8] L.Branchini, H. Perez-Blanco, Computing Gas Turbine Fuel Consumption To Firm Up Wind Power, Proceedings of ASME Turbo Expo 2012, June 11 – 12, 2012, Copenhagen, Denmark, Vol. 6, 2012, PP. 735-741, Doi: 10.1115/GT2012-68046

[9] M. Bianchi, L. Branchini, N. Cavina, A. Cerofolini, E. Corti, A. De Pascale, V.Orlandini, F. Melino, D. Moro, A. Peretto, F. Ponti, Managing wind variability with pumped hydro storage and gas turbines, 68th Conference of the Italian Thermal Machines Engineering Association, ATI2013, Bologna, 11-13 Sept. 2013, Energy Procedia, Vol. 45, 2014, pp. 22-31., Doi:10.1016/j.egypro.2014.01.004

[10] M. Bianchi, L. Branchini, N. Cavina, A. Cerofolini, A. De Pascale, F. Melino, Wind-hydro-gas turbine unit commitment to guarantee firm dispatchable power, Proceedings of the ASME Turbo Expo 2014, Dusseldorf; Germany; 16 - 20 June, 2014, Vol. 3B, Doi:10.1115/GT2014-25049

[11] M. Bianchi, L. Branchini, C. Ferrari, F. Melino, Optimal sizing of grid-independent hybrid photovoltaic–battery power systems for household sector, Proceedings of ICAE 2013, Fifth International Conference on Applied Energy, ICAE2013-336, Pretoria, South Africa, 1-4 July 2013

[12] M. Bianchi, L. Branchini, A. De Pascale , F. Melino, Storage Solutions for Renewable Production in Household Sector, Proceedings of ICAE 2014, 6th International Conference on Applied Energy, ICAE 2014; Taipei, Taiwan; 30 May - 2 June 2014; Energy Procedia, 2014, Vol. 61, pp. 242-245, Doi:10.1016/j.egypro.2014.11.1098

[13] G. Ple β mann, M. Erdmann, M. Hlusiak, C. Breyer, Global energy storage demand for a 100% renewable electricity supply, Energy Procedia, Vol. 46, 2013, pp. 22–31

[14] H. Chen, T.N. Cong, W. Yang, C. Tan, Y. Li, Y. Ding, Progress in electrical energy storage system: a critical review, Progress in Natural Science, vol. 19, 2009, pp. 291–312

[15] H. Ibrahim, A. Ilinca, J. Perron, Energy storage systems – characteristics and comparisons, Renewable Sustain Energy Reviews, vol. 12, 2007, pp. 1221–1250

[16] D.O. Akinyele, R.K. Rayudu, Review of energy storage technologies for sustainable power networks, Sustain Energy Technology Assess, vol. 8, 2014, pp. 74–91

[17] S. Koohi-Kamali, V.V. Tyagi, N.A. Rahim, N.L. Panwar, H. Mokhlis, Emergence of energy storage technologies as the solution for reliable operation of smart power systems: a review, Renewable Sustain Energy Reviews, vol.25, 2013, pp. 135–165

[18] S. Hameer, J.L. van Niekerk, A review of large-scale electrical energy storage, International Journal Energy Research, vol.39 , 2015, pp. 1179–1195,

[19] X. Luo, J. Wang, M. Dooner, J. Clarke, Overview of current development in electrical energy storage technologies and the application potential in power system operation, Applied Energy, vol. 137, 2015, pp. 511–536

[20] N.S. Pearre, L.G. Swan, Technoeconomic feasibility of grid storage: mapping electrical services and energy storage technologies, Applied Energy, vol. 137, 2015, pp. 501–510

[21] M. Castañeda, A. Cano, F. Jurado, , H. Sánchez, , L. M. Fernández, Sizing optimization, dynamic modeling and energy management strategies of a stand-alone PV/hydrogen/battery-based hybrid system, International Journal of Hydrogen Energy, Volume 38, Issue 10, 2013, Pages 3830–3845, DOI: 10.1016/j.ijhydene.2013.01.080

[22] D. Ipsakisa, S. Voutetakisa, P.Seferlisa, F. Stergiopoulos , C. Elmasides, Power management strategies for a stand-alone power system using renewable energy sources and hydrogen storage, Journal of Hydrogen Energy, Volume 34, Issue , 2009, Pages7081–7095, doi:10.1016/j.ijhydene.2008.06.051

[23] R.Carapellucci, L. Giordano, Modeling and optimization of an energy generation island based on renewable technologies and hydrogen storage systems, international journal of hydrogen energy, Volume 37, 2012, pages: 2081 -2093, doi:10.1016/j.ijhydene.2011.10.073

[24] K. Zhoua, J.A. Ferreira, S.W.H. de Haan, Optimal energy management strategy and system sizing method for stand-alone photovoltaic-hydrogen systems, Volume 33, 2008, pages: 477– 489, doi:10.1016/j.ijhydene.2007.09.027

[25] B. Guinota, B. Champela, F. Montignaca, E. Lemairea, D. Vannucci, S. Saillera, Y.Bultela, Techno-economic study of a PV-hydrogen-battery hybrid system for off-grid power supply: Impact of performances' ageing on optimal system sizing and competitiveness, International Journal of Hydrogen Energy, Volume 40, Issue 1, 2015, Pages 623–632, DOI: 10.1016/j.ijhydene.2014.11.007

[26] S.G. Tesfahunegn, Ø. Ulleberg, P.J.S. Vie, T.M. Undeland, Optimal shifting of Photovoltaic and load fluctuations from fuel cell and electrolyzer to lead acid battery in a Photovoltaic/hydrogen standalone power system for improved performance and life time, Journal of Power Sources, vol. 196, pp. 10401-10414, 2011.

[27] Mohammad Sadigh Behzadi, Mohsen Niasati, Comparative performance analysis of a hybrid PV/FC/battery stand-alone system using different power management strategies and sizing approaches, International Journal of Hydrogen Energy, vol. 40, pp. 538-548, 2015.

[28] Ø. Ulleberg, The importance of control strategies in PV–hydrogen systems, Solar Energy, vol. 76, pp. 323-329, 2004.

[29] R.E. Clarkea, S. Giddeya, F.T. Ciacchi, S.P.S. Badwal, B. Paulb, J. Andrews, Direct coupling of an electrolyser to a solar PV system for generating hydrogen, International Journal of Hydrogen Energy, vol. 34, pp. 2531-2542, 2009.

[30] E. Dursun, B. Acarkan, O. Kilic, Modeling of hydrogen production with a stand-alone renewable hybrid power system, Int J Hydrogen Energy, 37 (2012), pp. 3098–3107

[31] Mehmed Eroglu, Erkan Dursun, Suat Sevencan, Junseok Song, Suha Yazici, Osman Kilic, A mobile renewable house using PV/wind/fuel cell hybrid power system, Int J Hydrogen Energy, 36 (2011), pp. 7985–7992

[32] M. Santarelli, M. Calì, S. Macagno, Design and analysis of stand-alone hydrogen energy systems with different renewable sources, Int J Hydrogen Energy, 29 (2004), pp. 1571–1586

[33] B. Escobar, J. Hernández, R. Barbosa, Y. Verde-Gómez, Analytical model as a tool for the sizing of a hydrogen production system based on renewable energy: the Mexican Caribbean as a case of study, Int J Hydrogen Energy, 38 (2013), pp. 12562–12569.

[34] V.M. Sanchez, A.U. Chavez-Ramirez, S.M. Duron-Torres, J. Hernandez, L.G. Arriaga, J.M. Ramirez, Techno-economical optimization based on swarm intelligence algorithm for a stand-alone wind-photovoltaic-hydrogen power system at south-east region of Mexico, Int J Hydrogen Energy, 39 (2014), pp. 16646–16655.

[35] L.G. Arriaga, W. Martinez, U. Cano, H. Blud, Direct coupling of a solar-hydrogen system in Mexico, Int J Hydrogen Energy, 32 (2007), pp. 2247–2252.

[36] Yunez-Cano, R. de G. González-Huerta, M. Tufiño-Velázquez, R. Barbosa, B. Escobar, Solar-hydrogen hybrid system integrated to a sustainable house in Mexico, Int J Hydrogen Energy, 41 (43) (2016), pp. 19539–19545.

[37] Heckert Solar, Polycrystalline PV module nemo ®54 P, http://www.heckertsolar.com/en/products/solar-modules/solar-module-nemor-54-p.html

[38] H. Fathabadi, Novel photovoltaic based battery charger including novel high efficiency step-up DC/DC converter and novel high accurate fast maximum power point tracking controller, Energy Conversion and Management, Vol. 110, 2016, pp. 200–211, doi:10.1016/j.enconman.2015.12.025

[39] Steca Elektronic, Steca PR 10-30 1010, 1515, 2020, 3030, http://www.steca.com/index.php?Steca-PR-10-30-en

[40] Yasser E. Abu Eldahab, , Naggar H. Saad, Abdalhalim Zekry, Enhancing the design of battery charging controllers for photovoltaic systems, Renewable and Sustainable Energy Reviews, Volume 58, 2016, pp. 646–655, doi:10.1016/j.rser.2015.12.061

[41] Banner Batterien, SBV 12-18 → SBV 12-250, http://www.bannerbatterien.com/banner/files/FolderSBVBlocD_2015.pdf

[42] Meanwell, SD-25B-12 and TS-700-224B manual, http://www.meanwell.com/mw_search/sd-25/sd-25-spec.pdf and http://www.meanwell.com/mw_search/TS-1000/TS-700,1000-E.pdf

[43] Heliocentris, Solar Hydrogen Extension Mobile unit for Solar Hydrogen Production, http://shecey.com/wp-content/uploads/2015/09/Solar-Hydrogen-Extension_Brochure_EN_1106.pdf

557    **APPENDIX A**

558

**Table**

1    **APPENDIX A**

2    **Table A1:** Solar Module technical specifications [21]

| DESIGNATION | SPECIFICATION |
|---|---|
| Type | Polycrystalline PV Module NeMo® 54 P |
| Max. power | 220 W (@NOCT: 155 W) |
| Rated voltage | 24 V |
| Open circuit voltage ($V_{OC}$) | 33.77 V (@NOCT: 30.41 V ) |
| MPP voltage ($V_{MPP}$) | 27.54 V (@NOCT 23.40 V ) |
| MPP current ($I_{MPP}$) | 8.08 A (@NOCT 6.62 A) |
| Short circuit current ($I_{SC}$) | 8.62 A (@NOCT 7.02 A) |
| Max. system voltage | 1,000 V |
| Dimensions | 990 mm x 1,480 mm x 38mm |
| Weight | 19 kg |
| Reliability | 10 years 90 %, 25 years 80 % |
| Quantity | 2 units |
| Short Circuit Current Temperature coefficient | 0.05%/K |
| No-load Voltage Temperature coefficient | -0.32%/K |
| Performance coefficient | -0.42%/K |

3    **Table A2:** solar charge regulator technical specifications [23]

| DESIGNATION | SPECIFICATION |
|---|---|
| Type | PWM-PR3030 |
| System voltage | 12 V (24 V) |
| Own consumption | 12.5 mA |
| Open circuit voltage solar module | < 47 V |
| Module current | 30 A |
| Load Current | 30 A |
| End of charge voltage | gel 14.1 V (28.2V) |
| Boost charge voltage | 14.4 V (28.8 V) |
| Equalisation charge | 14.7 V (29.4 V) |
| Reconnection voltage (SOC/LVR) | > 50% /12.6 V (25.2 V) |
| Deep charge protection (SOC/LVD) | < 30% / 11.1 V (22.2 V) |
| Ambient temperature operating conditions | -10°C…. +50°C |
| Terminal (fine/single wire) | 16 mm$^2$/25 mm$^2$    AWG 6/4 |
| Degree of protection | IP 32 |
| Dimensions (XxYxZ) | 187 x 96 x 44 |
| Weight | 350 g |

4    **Table A3:** Battery technical specifications @ambient temperature 20 °C [25]

| DESIGNATION | | | SPECIFICATION |
|---|---|---|---|
| Type | | | Gel SBV 12-55 |
| Capacity | C 20 | 1.8 V/C | 55 Ah |
| Rated voltage | | | 12 V |
| Internal resistance | | | 7.5 mOhm |
| Compensation charge voltage | | | 2.27 V/cell |
| Operating temperature | | | -10 °C……40°C |
| Dimensions (L x W x H) | | | 228 mm x 137mm x 210 mm |
| Weight | | | 17.7 kg |
| Quantity | | | 2 units |

5

6    **Table A4:** DC/DC converter and DC/AC inverter technical specifications [26]

| DC/DC CONVERTER | |
|---|---|
| DESIGNATION | SPECIFICATION |

| Type | Meanwell SD-25B-12 |
|---|---|
| Output Voltage | 12V DC |
| Input Voltage Range | 19→36 V DC |
| Input Nominal Voltage | 24 V DC |
| Isolation Voltage | 1500 V AC |
| Power Rating | 25.2 W |
| Rated efficiency | 78 % |
| Output Current | 2.1 A |
| Mounting Type | Chassis Mount |
| Number of Outputs | 1 |
| Temperature range | -10°C….+60°C |
| Length/depth/width | 99mm/36mm/97mm |
| **DC/AC INVERTER** | |
| **DESIGNATION** | **SPECIFICATION** |
| Type | Meanwell TS-700-224B |
| Output Voltage | 230 V AC |
| Input Voltage Range | 21      30V DC |
| Input current | 38 A |
| Rated power | 700 W |
| Rated efficiency | 90 % |
| Working temperature | 0 ~ +40 @ 100% load ; +60 @ 50% load |
| DIMENSION | 295*184*70mm (L*W*H) |

**Table A5:** Hydrogen generator technical specifications [27]

| **HYDROGEN GENERATOR** | |
|---|---|
| **DESIGNATION** | **SPECIFICATION** |
| Type | PEM |
| Production rate | 30 sl/h at 10.7 bar |
| Hydrogen quality | 6.0 (99.9999 %) |
| Power consumption | 300/600 VA |
| Dimensions (W x H x L) | 230 x 355 x 410 mm |
| **METAL HYDRIDE CANISTERS** | |
| **DESIGNATION** | **SPECIFICATION** |
| Type | Metal hydride OV555 |
| Capacity | 200 sl (each) |
| Hydrogen quality | 5.0 (99.999%) |
| Output | 1.5 sl/min |
| Charge pressure | 10…17 bar |
| Dimensions (W x H x L) | Ø 89 x 420 mm |
| Weight | 14.33 lb |
| Quantity | 3 |

**Table A6:** Average, standard deviation and variance values of the dimensionless parameters $I_{MPP}/I$, $V_{MPP}/V$ and $P_{MPP}/P$ for the tests conducted on solar panels.

| | Average [-] | | | Standard Deviation [-] | | | Variance [-] | | |
|---|---|---|---|---|---|---|---|---|---|
| Test | $I_{MPP}/I$[-] | $V_{MPP}/V$[-] | $P_{MPP}/P$[-] | $I_{MPP}/I$[-] | $V_{MPP}/V$[-] | $P_{MPP}/P$[-] | $I_{MPP}/I$[-] | $V_{MPP}/V$[-] | $P_{MPP}/P$[-] |
| #1 | 0.7857 | 1.004 | 1.5663 | 0.9581 | 0.0427 | 1.9416 | 0.9180 | 0.0018 | 3.77 |
| #2 | 0.6531 | 1.0422 | 1.3574 | 0.111 | 0.0187 | 0.2071 | 0.0123 | 0.0004 | 0.0429 |
| #3 | 0.5302 | 1.0637 | 1.1278 | 0.0156 | 0.0058 | 0.0281 | 0.0002 | 3.42e-05 | 0.0008 |
| #4 | 0.5772 | 1.0173 | 1.2171 | 0.0401 | 0.0144 | 0.0720 | 0.0016 | 0.0002 | 0.0052 |
| #5 | 0.5039 | 0.9773 | 0.985 | 0.0217 | 0.0063 | 0.0453 | 0.0005 | 3.95e-05 | 0.0020 |
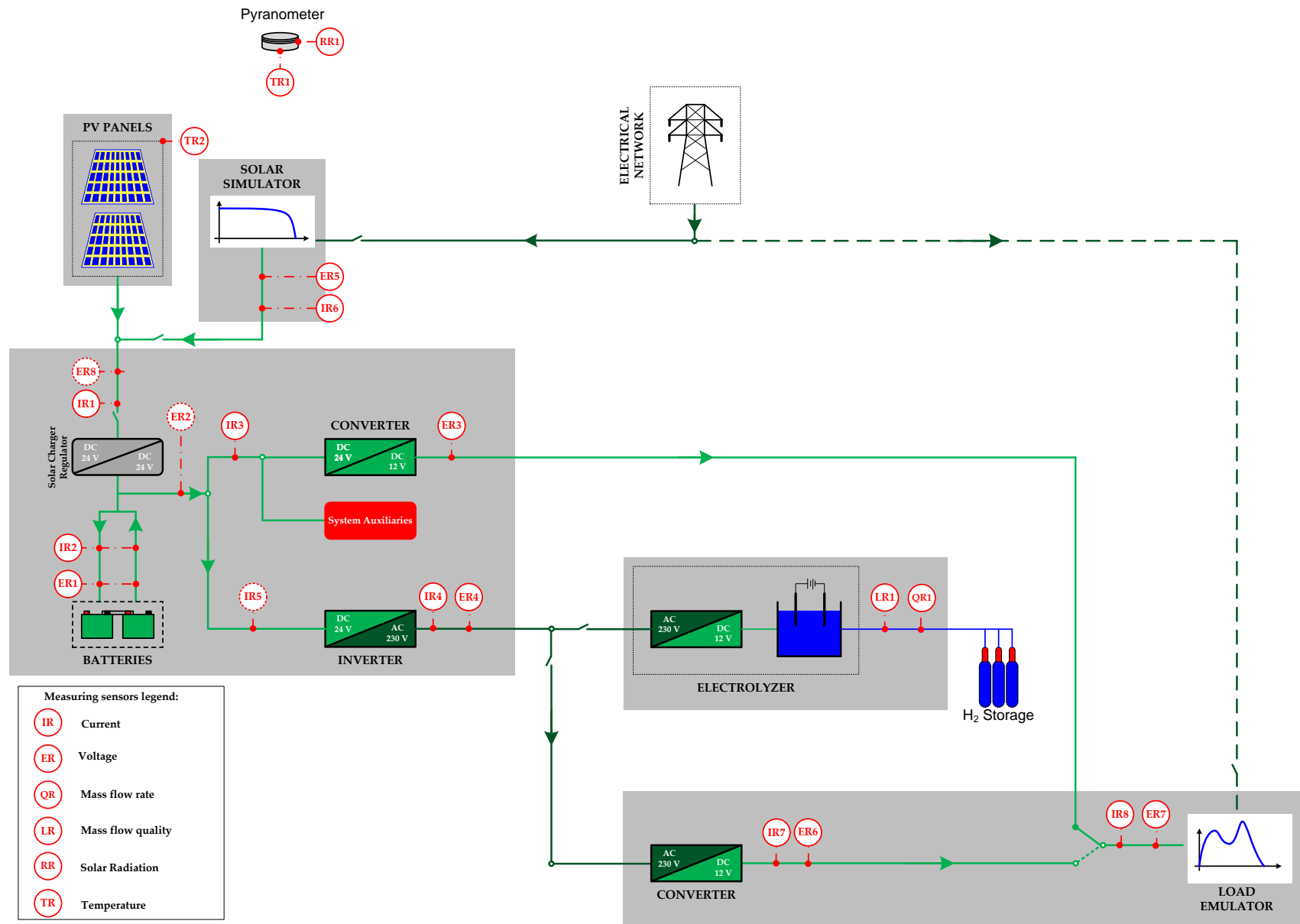
**Figure**



**Figure 1:** Schematic layout of the integrated laboratory microgrid with installed measuring sensors

| Solar modules | Power management cabinet | Hydrogen generator & data acquisition system |
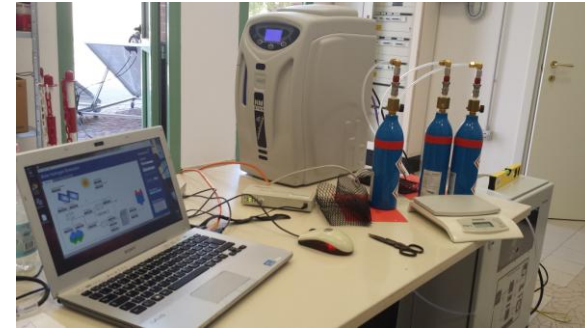
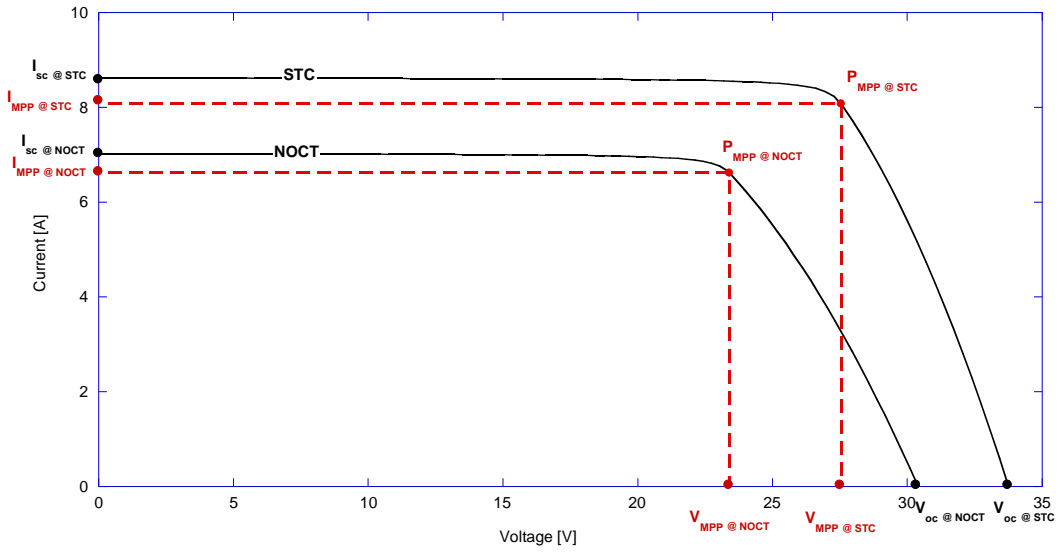**Figure 2:** The "*microgrid and storage*" laboratory test facility

**Figure 3**: I-V curves at STC and NOCT conditions, based on manufacturer specifications [26] (see Table A1 Appendix A).
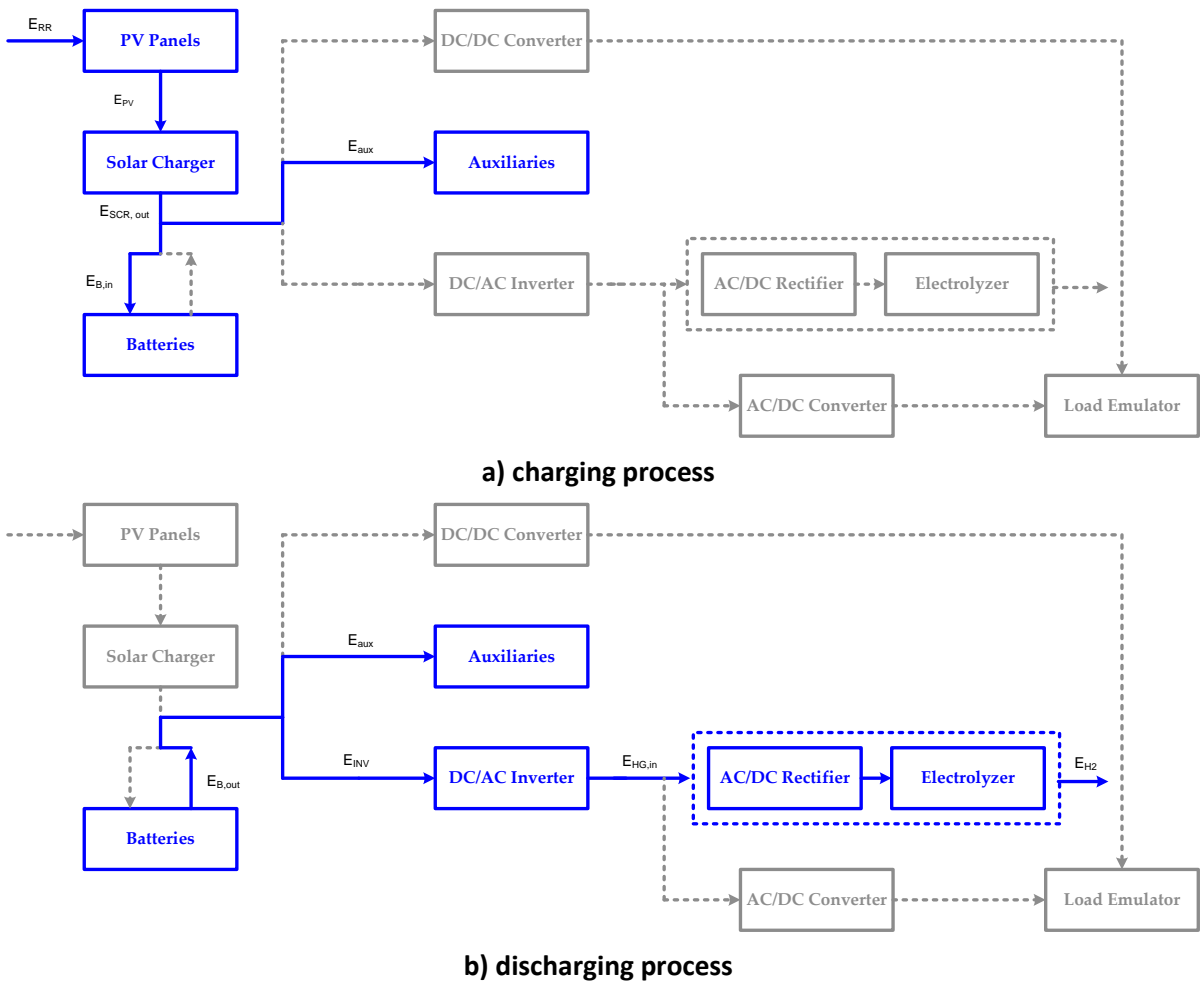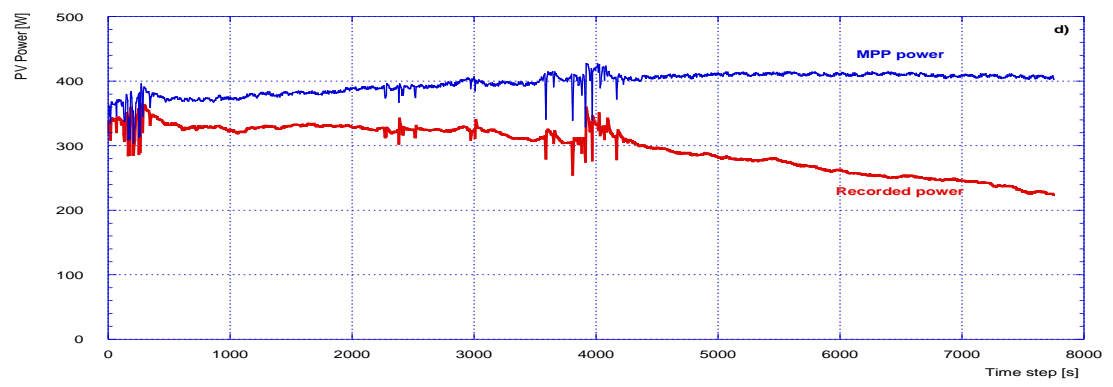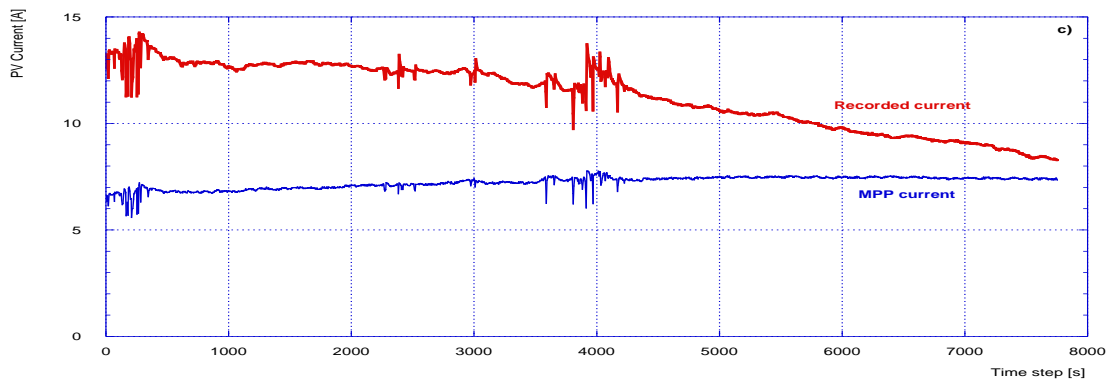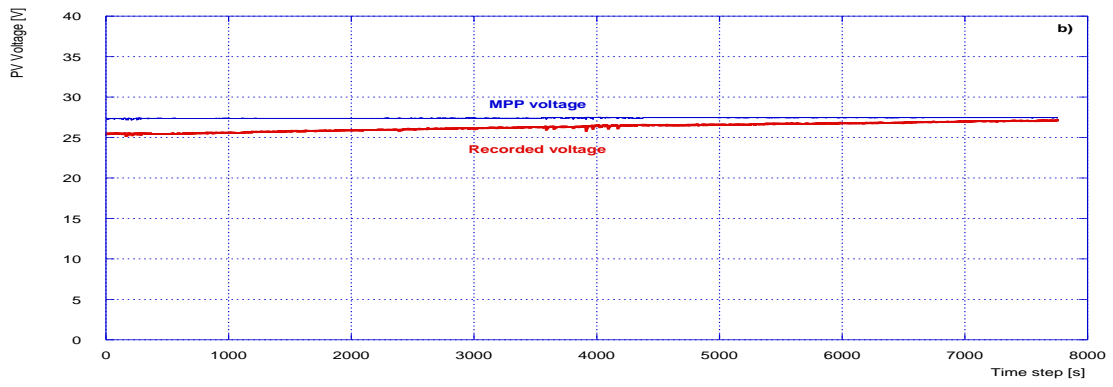


**a) charging process**



**b) discharging process**

**Figure 4:** schematic of energy fluxes inlet/outlet from each microgrid component (investigated process is highlighted with continuous blue lines) a) charging b) discharging processes

17

18

19

20
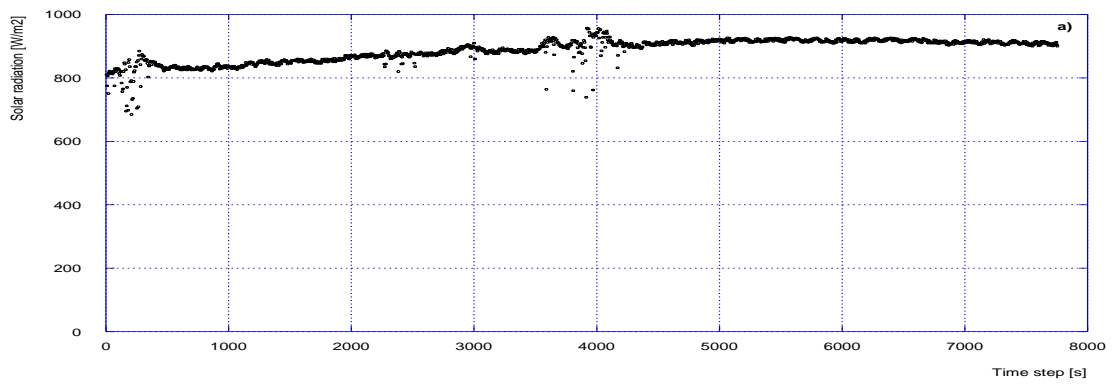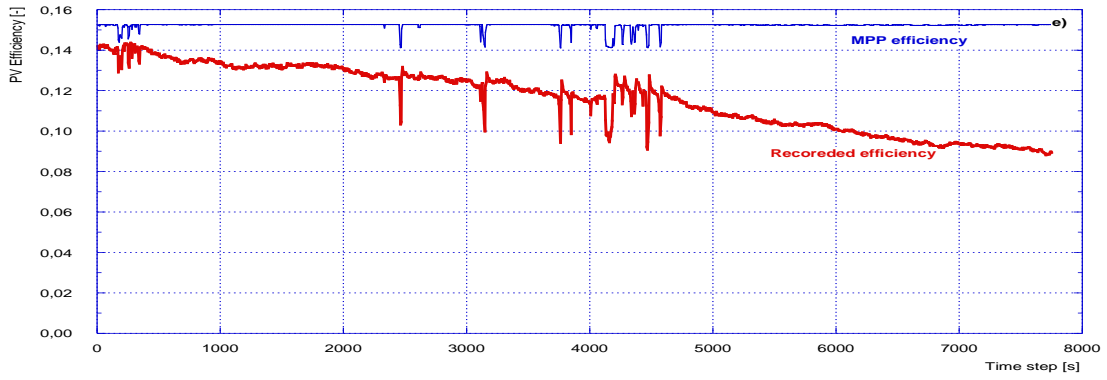
**Figure 5:** a) Solar Radiation values recorded, b) MPP and recorded panels voltage; c) MPP and recorded panels current; d) MPP and calculated panels power production; e) MPP and calculated panels efficiency.
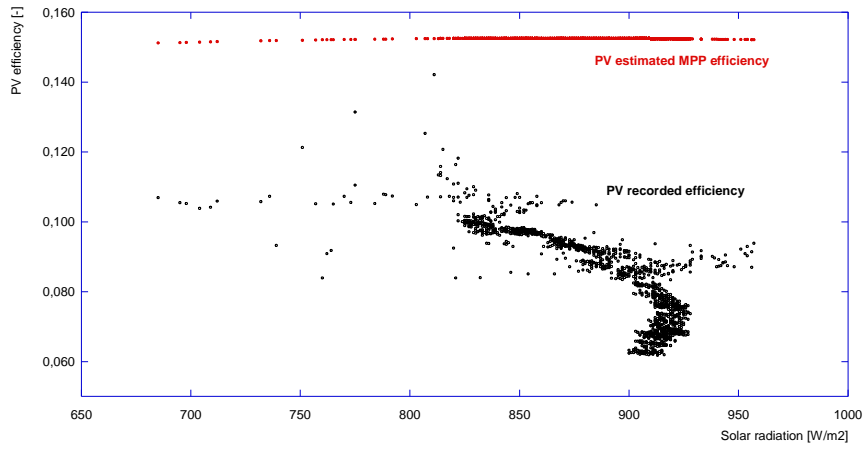


**Figure 6:** PV estimated MPP and recorded efficiencies as function of different solar radiation values.
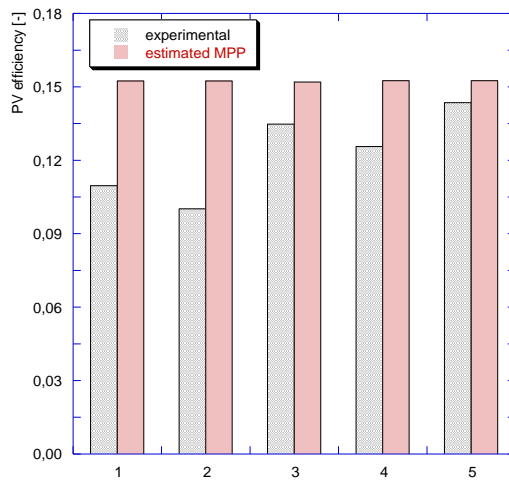


**Figure 7:** PV experimental and MPP efficiency values for five experimental batteries **charging** tests.
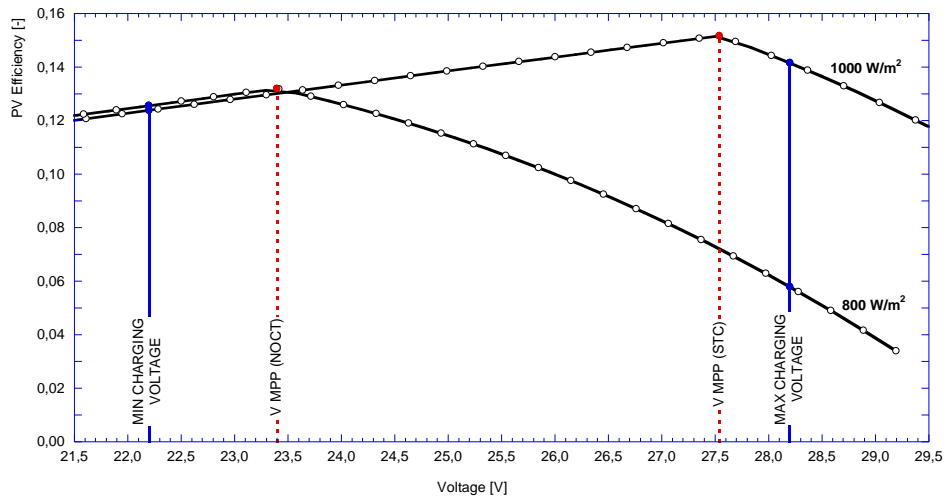
**Figure 8:** PV efficiency behavior versus voltage for two solar radiation values (1000 and 800 W/m$^2$ ).
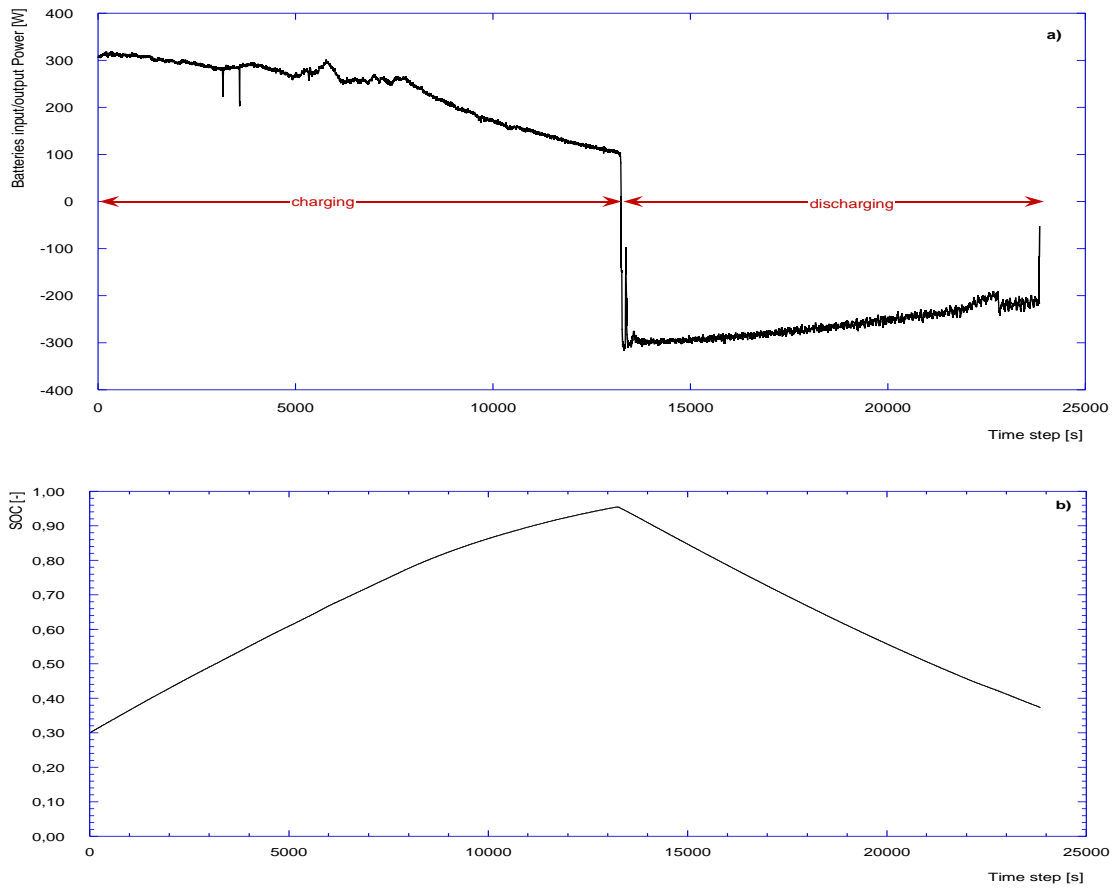


**Figure 9:** a) Input/output power recorded to/from batteries; b) calculated batteries SOC during a charging/discharging test.
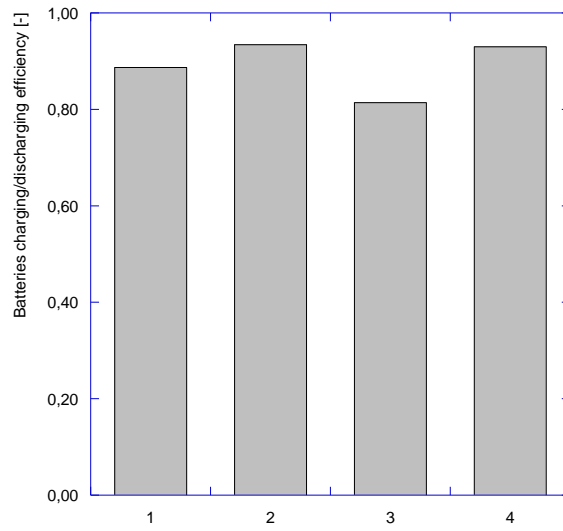
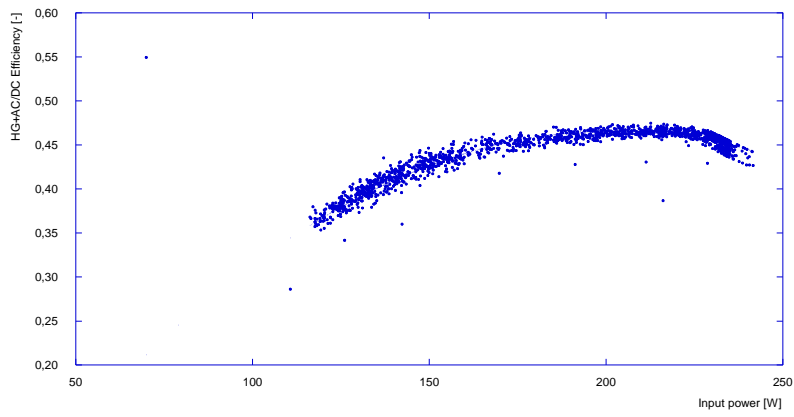**Figure 10:** batteries charging/discharging efficiency values obtained for four different experimental tests.



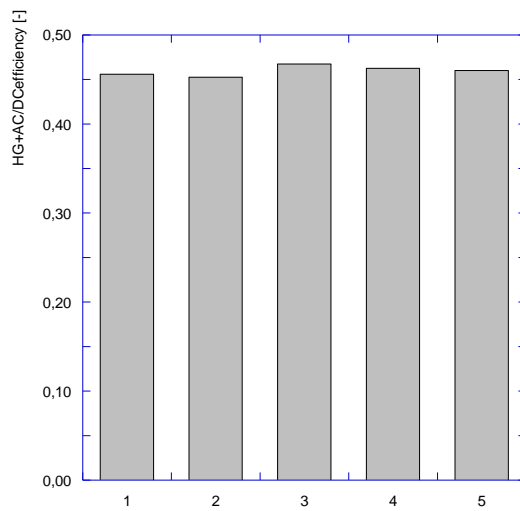**Figure 11:** efficiency of the HG+AC/DC component as function of input power.



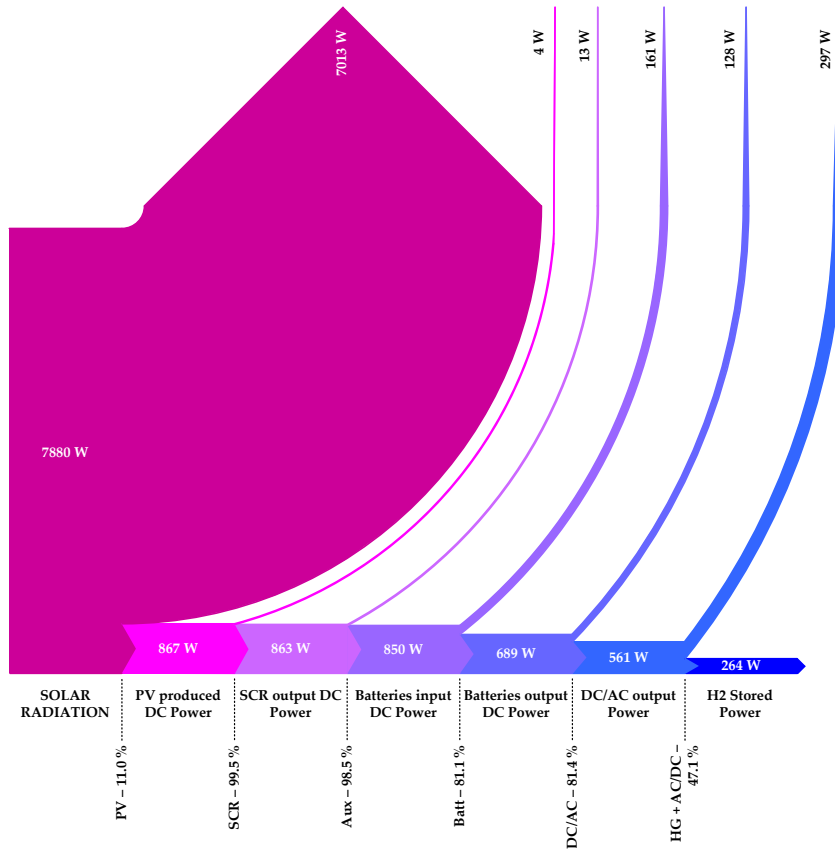**Figure 12:** HG+AC/DC efficiency values for five different tests.

# LOSSES



**Figure 13:** Overall solar-hydrogen generation chain.

51
52
53

**LaTeX Source Files**

Click here to download LaTeX Source Files: journal_hydrogen_FINAL_CLEAR.doc